2022 International Symposium on Power Electronics, Electrical Drives, Automation and Motion (SPEEDAM) | 978-1-6654-8459-6/22/$31.00 ©2022 IEEE | DOI: 10.1109/SPEEDAM53979.2022.9841972

Impact of PLL Design on Data-Driven Models for Grid-Connected Single-Phase Inverters

Sunil Subedi†, Robert Fourney,
Hossein Moradi Rekabdarkolaee,
Reinaldo Tonkoski, and Timothy M. Hansen
South Dakota State University
Brookings, South Dakota, USA
Email: †sunil.subedi@jacks.sdstate.edu

Jesus D. Vasquez-Plaza and
Fabio Andrade
University of Puerto Rico, Mayaguez
Mayaguez, Puerto Rico, USA

***Abstract*—This paper investigates the impact of quadrature signal generation based phase-locked loop (QSG-PLL) methods on data-driven modeling of grid-connected single-phase inverters (GCSI). The magnitudes of the grid voltage and current injected by a GCSI simulated in MATLAB/Simulink are estimated by each QSG-PLL approach. The best transfer function for the GCSI model is estimated in terms of goodness of fit, using the magnitudes obtained by each approach and the instrument variable system identification approach. Different grid disturbances (e.g., voltage sag, phase angle jumps, harmonic distortions, frequency fluctuation) are used to evaluate the performance of each data-driven model in comparison to the simulated model. The paper provides researchers guidance on which QSG-PLL to use to model GCSIs using data-driven methods.**

***Index Terms*—Data-driven, phase-locked loop, quadrature signal generation, single-phase inverter, systems identification.**

I. Introduction

The high penetration of distributed energy resources (DERs) are causing a paradigm shift from a traditionally passive to more dynamic system [1]. Modern grid codes, e.g., IEEE 1547-2018, have been issued and new grid-connected single-phase inverters (GCSI) with grid support functions (GSF) have been developed. The installation of such devices facilitate the integration of additional converter-based DERs to regulate grid voltage and frequency, preserving grid stability, and increasing grid dependability. Moreover, commercial off-the-shelf grid-connected inverters operate as grid-following sources and operate by following the grid frequency/angle in real-time. Thus, to enhance the nominal operation of the grid-tied system and provide ancillary grid services, smart inverters with GSFs need to quickly estimate the grid phase, amplitude, and frequency to inject synchronized grid currents with excellent power quality [2].

System operators and researchers use simulation and modeling platforms to better understand the dynamics of converter dominated power systems (CDPS); poor modeling can result in inaccurate data and analysis, making proper system operation and planning difficult. For accurate modeling of such non-linear systems, a thorough understanding of the converter is essential, yet extracting exact dynamics becomes difficult as the topology and/or control strategies vary across the vendor models. To address the aforementioned challenges, black-box or data-driven models are popular in modeling the GCSI in CDPS. The instantaneous voltage at the point of common coupling (PCC) and the output current of an inverter are used to create a data-driven model of a grid-tied converter [3]. Peak voltage detection, root mean square (RMS), and discrete Fourier transform techniques are employed to obtain peak current and voltage amplitude. However, due to their slow dynamics and half-cycle time delays, these approaches provide non-instantaneous peak values [2]. Quadrature signal generator with synchronous reference frame phase-locked loop (QSG-SRF-PLLs) are popular for extracting voltage and current amplitude along with the synchronization and control of GCSI due to the ease of implementation and satisfactory performance in solving the aforementioned problems.

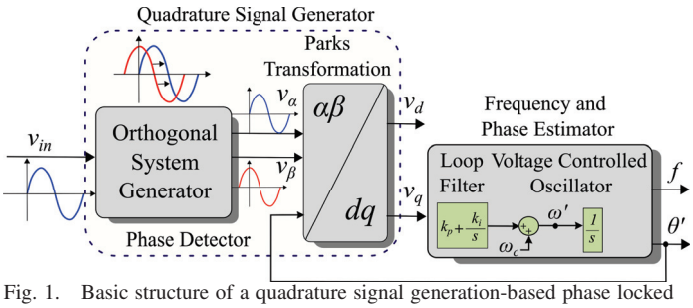

Fig. 1. Basic structure of a quadrature signal generation-based phase locked loop (QSG-PLL) system.

In general, PLLs have three building blocks namely phase detector (PD), loop filter (LF), and voltage controlled oscillator (VCO) [4]. Because of the impact of PD on filtering need and dynamic response of these PLLs in the event of grid disturbances (e.g., voltage sag, phase angle jumps (PAJ), harmonics distortions, and frequency variation (FV)), PD block implementation has gained a lot of attention especially in single-phase PLLs [5]. Fig. 1 shows the general structure of a single-phase PLL system with QSG as PD.

PLLs with different PD control structures and properties are used at different levels of the power system. QSG-based PLLs with the second-order generalized integral (SOGI), inverse

This work is supported by the U.S. Department of Energy Office of Science, Office of Electricity Microgrid R&D Program, and Office of Energy Efficiency and Renewable Energy Solar Energy Technology Office under the EPSCoR grant number DE-SC0020281.

parks transform (IPT), all-pass filter (APF), and sliding Fourier transform (SFT) are found to perform better in solving the aforementioned problems. They are commonly used in the construction of the PD block of single-phase PLLs due to their low computational weight, high filtering capability, resilient performance, and relatively fast transient response [6]. While most prior research has ignored the impacts of PLL dynamics while modeling GCSIs with data-driven approach, a few have considered them in their study [7]. However, little study and analysis has been conducted on the impact of PLL dynamics utilized for grid detection on black-box models of GCSIs using the system identification technique, as the precision of the generated linear dynamic models is dependent on peak measurements and synchronization. Therefore, the objectives of this study are to investigate the influence of various QSG-PLL designs utilized for instantaneous grid measurement in GCSI, as well as to assist researchers in analyzing and guiding the selection of PLLs in system-level analysis for black-box modeling. Under non-ideal system conditions (such as frequency and amplitude fluctuations, phase jump, harmonics etc.), a complete assessment of QSG-PLL algorithms is performed by developing a reduced-order transfer function (TF) model, and theoretical and simulation research findings are presented.

The rest of the paper is structured as follows. The detailed GCSI system under investigation and the system identification algorithm for deriving the TF model of that system with selected PLLs is discussed in Section II. Section III gives the theoretical insights of basic structure and the working principles of each of the PLLs. Then, the performance evaluation of the selected PLLs based on simulation findings followed by the derivation of black-box models of GCSI with different PLLs and their impact on developed models is presented in Section IV. The main conclusions from this study are presented in Section V.

II. Dynamic Modeling of Inverter-Based Generator

The converter system considered in this study is depicted in Fig. 2, which consists of an 8.4 kW switched single-phase voltage source inverter powered by a constant DC bus and coupled to the main grid via an LCL filter to attenuate switching noise. Input current, capacitor voltage, output current, and grid voltage are defined as I_i, V_c, I_o, and V_g, respectively.

In the dq framework, a proportional-integral (PI) controller was used to regulate the current injected to the main grid by the voltage source inverter. To generate the reference current based on power references, the PQ controller block is used. The same QSG block was used to create the I_o and V_g quadrature signals used by the PI and PQ controllers blocks for all experiments. In practice, the PLL used for synchronization within the SGCI is hidden. However, for the purposes of our detailed model, we will assume that the synchronization PLL is the same as the PLL used for grid detection. The grid detecting unit (QSG-PLL) and the converter PLL in Fig. 2 were replaced by QSG techniques indicated in Section III,

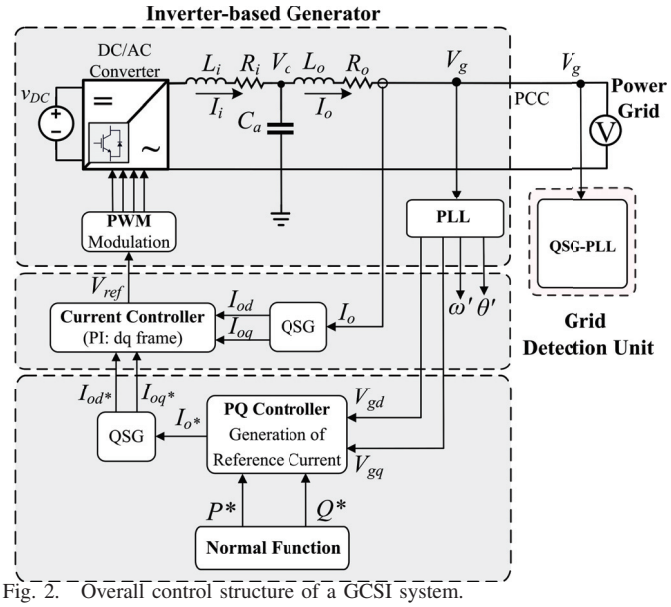

Fig. 2. Overall control structure of a GCSI system.

predicting the fundamental frequency, angle, and amplitude of the system used by the inner QSGs. The construction of the mathematical model of the GCSI dynamics was generated for each QSG method from output (I_o) and input (V_g) using the system identification algorithm with the instrument variable approach, which is detailed in [3]. The goodness of fit between the test and reference output from mathematical models with varying pole and zero are evaluated as stated in (1). The ratio in the equation is the Normalized Root Mean Square Error (NRMSE), and $y(t)$ and $\hat{y}(t)$ are the data from the detailed inverter and linear TF simulation model, respectively [3]. The performance and impact of each QSG method are discussed in Section IV.

$$fit = 100 \times \left[1 - \frac{\|y(t) - \hat{y}(t)\|_2}{\|y(t) - \bar{y}(t)\|_2}\right] \quad (1)$$

The specifications of the single-phase voltage inverter with full-bridge topology are listed in Table I for simulation tests.

TABLE I
Parameters of GCSI system.

Parameter	Value
Nominal RMS voltage amplitude	V_{RMS} = 120 V
Fundamental frequency	ω_c = 377 rad/s
Switching frequency	f_{sf} = 10 kHz
Sampling Time	T_s = 100 µs
DC bus voltage (V_{DC})	400 V
LCL Filter (L_i=L_o, R_i=R_o, C_a)	1.8mH, 0.1Ω, 8.8μF
PI Controller (K_p, K_i)	4.5, 60

III. Grid Synchronization in GCSI

The application of Clark's and Park's transformation is beneficial in three-phase transformation-based PLLs; however, in a single-phase system, the PLL structure is more complicated due to the presence of a single input signal [8]. The actual signal and the produced fictitious orthogonal signal, which are considered comparable $\alpha-\beta$ quantities, are obtained using

QSG-PLL in conjunction with an orthogonal system generator, and thus an SRF transformation based PLL is applied to single-phase systems. This section explains the working principles and general structure of the selected four typical PLL systems based on the above PD techniques. The PLL parameters are derived from [4], [6], which provide a complete systematic design approach and comprehensive review of each PLL. However, the design of the PLLs and their parameters is beyond the scope of this article.

A. Second Order Generalized Integrator (SOGI)-based PLL

SOGI converts a single-phase alternating current (AC) signal into an orthogonal signal without delay. The α-axis component is a filtered input signal of the main grid's voltage and current, and the resulting β-axis component is displaced $90°$ from the original components with the same amplitude to achieve orthogonality. The block diagram of the general SOGI-PLL system is shown in Fig. 3, where calculated angular frequency (ω') is fed back into the PD. Only the control parameter k influences the bandwidth and dynamic response of the calculated output signals; $k = \sqrt{2}$ is found to be optimal. A detailed systematic design procedure is presented in [4].

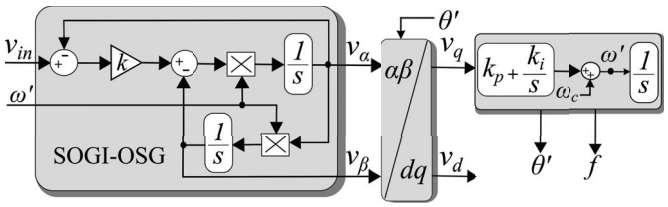

Fig. 3. Block diagram of a typical SOGI based QSG-PLL.

B. Inverse Park's Transform (IPT)-based PLL

The IPT is made up of two blocks called ($dq \rightarrow \alpha\beta$) and ($\alpha\beta \rightarrow dq$). IPT is applied to the filtered direct and quadrature signals to produce the needed orthogonal signal and direct outputs are fed back via two low pass filters (LPF), as shown in Fig. 4. This approach is simple to use, but dynamics mainly depend on the characteristics of the LPF, therefore it necessitates precise adjustment of LPF parameters. For simplicity and to eliminate the in-loop phase delay, first-order infinite impulse response (IIR) LPFs are most typically used.

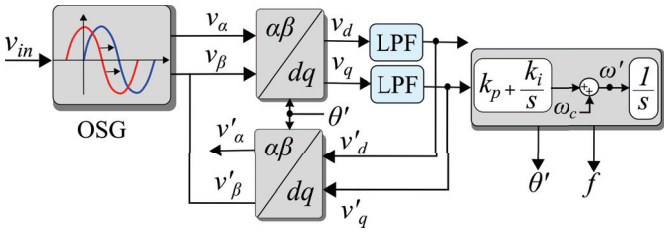

Fig. 4. Block diagram of a typical IPT based QSG-PLL.

C. All-pass Filter (APF)-based PLL

The conventional APF-PLL creates quadrature signals using a first-order APF of the form $(\omega' - s)/(\omega' + s)$, as illustrated in Fig. 5. The APF receives the estimated frequency ω' to adjust to grid frequency changes. An APF is developed by designing a Kalman-based filter and selecting the necessary gains (k_e and k_f). The value of k_e must be equal to $-k_f$ to establish the two orthogonal axes.

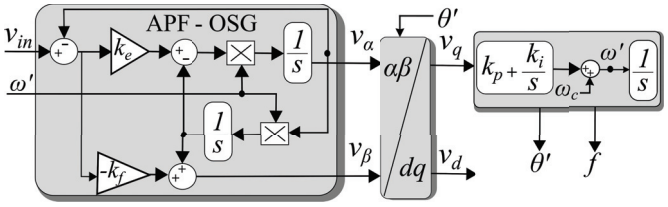

Fig. 5. Block diagram of a typical APF based QSG-PLL.

D. Sliding Fourier Transform (SFT)-based PLL

The real and imaginary components of the SFT transfer function described in [4], which passes the fundamental component and rejects all other harmonics up to the aliasing point, can be utilized to generate the orthogonal signal. The sampling frequency is adjusted according to the fundamental frequency (ω_c) with N samples. SFT-PL is designed to track the frequency of the input signal, and the fluctuation in amplitude and frequency information can be retrieved from the PLL. Even though they are computationally efficient, they have limitations in non-ideal grid scenarios; however, there have been numerous advancements in the literature [4].

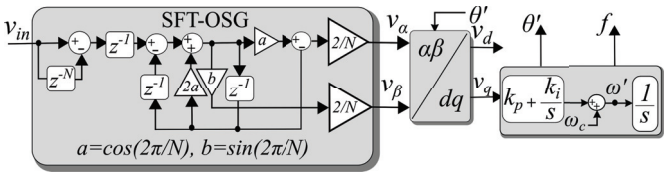

Fig. 6. Block diagram of a typical SFT based QSG-PLL.

IV. Performance Comparison of the PLLs and the Impact on Data-Driven Models

PLL uses the PCC voltage to identify the utility grid's phase angle in weak grid settings, and the PCC voltage connects the PLL and the current control loop when the grid current passes through the grid impedance, improving overall system performance. In this section, the impact of different PLLs under weak grid conditions on the GCSI system is discussed in detail. The derivation of the data-driven models for GCSI with each PLL and their impact on the developed models are then examined using MATLAB/Simulink.

A. Performance evaluation of QSG-PLLs

To make a fair comparison in the performance and see the impact of each PLL on data-driven models, all QSG-PLLs are designed with the same parameters, and selected parameters are shown in Table II. Voltage sag, FV, PAJ, and

harmonic distortion are the severe grid conditions used for this study. Fig. 7 shows the dynamics of the amplitude, estimated frequency, and phase-angle error from the simulation of four QSG-PLLs during 30% voltage sag at t = 0.15 s, +2 Hz FV at t = 0.3 s, −40° PAJ at t = 0.45 s, and distortion due to the harmonics (5% of 3^{rd} and 5^{th} harmonics) at t = 0.6 s [6].

TABLE II
CONTROL PARAMETERS FOR PLL.

Parameter	Value
Damping ratio for PI	$\zeta = 1/\sqrt{2}$
Proportional Gain (dq frame)	k_p = 92, k_i = 4232
Settling time	t_s = 100 ms
Cutoff frequency in IIR for IPT	f_c = 20 Hz
k in SOGI QSG	$\sqrt{2}$
k_f=-k_e in APF QSG	-1

The above-mentioned grid synchronization algorithms are compared using overshoot (OS in %) and settling time (t_s in ms) as the criteria. To investigate the impact of different PLLs in data-driven modeling, we primarily looked at voltage dynamics during grid events. The performance of PLLs in tracking the amplitude attributed to grid events is shown in the Table III. The SOGI-based QSG-PLL delivers the fastest response when compared to the other techniques, yet at a slightly higher OS during the 30% grid voltage sag event. Moreover, SOGI retains its faster dynamics in the estimated amplitude with minimal OS during the +2 Hz increase in frequency. With the step shift in frequency, SOGI maintains its quicker dynamics in the predicted amplitude with negligible OS. However, during the PAJ, SFT performed well followed by IPT, while OS for SOGI and APF is higher respectively.

TABLE III
AMPLITUDE DYNAMICS DURING EVENTS.

Grid Events	IPT		SOGI		SFT		APF	
	OS	t_s	OS	t_s	OS	t_s	OS	t_s
30% Sag	1.07	110	1.6	70	0.8	110	0.8	100
+2 Hz FV	0.84	120	0.75	100	1.93	125	2.45	110
−40° PAJ	11.7	130	16	100	6.5	110	21.8	120

B. Impact of QSG-PLLs on Data-driven Models of GCSI

A square wave of 20 Hz frequency with a regulated voltage source is used to perturb the system considering each QSG. A black-box model is trained using a square wave with an amplitude of 0.98 to 1.02 p.u, and the developed model is validated using a signal with an amplitude of 0.97 to 0.99 p.u. An RMS approach typically adds delay and has slower dynamics tracking the amplitude of the grid voltage and current as compared to the response from the QSGs.

The performance of the GCSI using SOGI-PLL as a synchronization unit and the RMS-block from MATLAB is shown in Fig. 9, which reveals that the RMS-block has a slower response while tracking grid voltage and output current amplitude during grid voltage changes. Model orders were varied to see if they could help with fit, however no substantial benefits were observed at the expense of additional model complexity. The best fit appears to be a second-order TF model with two poles and a single zero for experiments involving

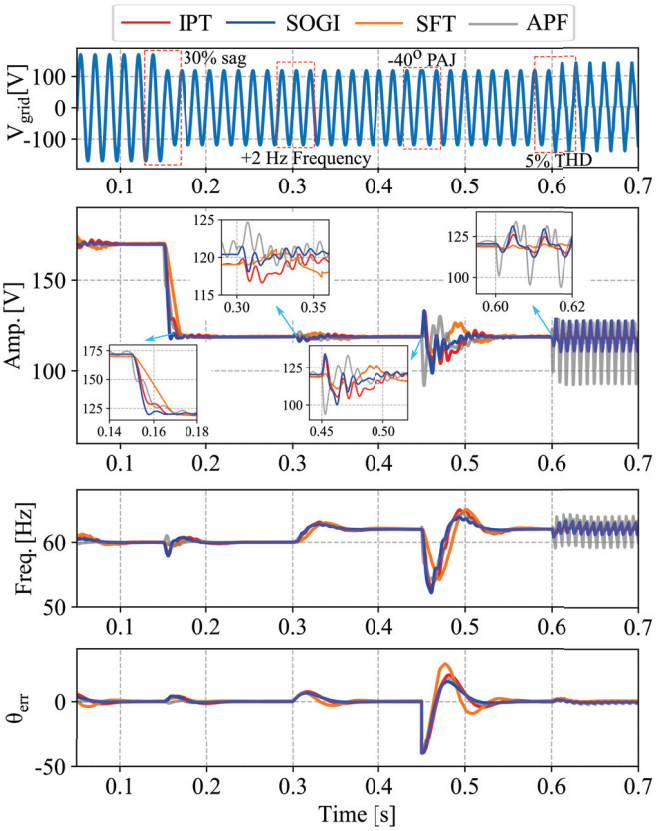

Fig. 7. Grid synchronization dynamics comparison during 30% sag at t = 0.15 s, −40° phase amplitude jump (PAJ) at t = 0.3 s, +2 Hz frequency variations (FV) at t = 0.45 s and grid voltage (third and fifth order) distortion having 5% THD at t = 0.6 s.

TABLE IV
A SUMMARY OF THE BEST TFS MODELS OBTAINED USING THE SYSTEM IDENTIFICATION ALGORITHM VARYING POLE AND ZERO.

Methods	Model Coefficients	Goodness of Fit to Training Data
IPT	b_1 = 415.7, b_0 = -1.43×10^5 a_2 = 1.000, a_1 = 724.4 a_0 = 2.462×10^5	97.33%
SOGI	b_1 = 341, b_0 = -1.368×10^5 a_2 = 1.000, a_1 = 671.8 a_0 = 2.253×10^5	98.23%
SFT	b_1 = -430.5, b_0 = -2602 a_2 = 1.000, a_1 = 463.6 a_0 = 4721	95.87%
APF	b_1 = 528.2, b_0 = -1.966×10^5 a_2 = 1.000, a_1 = 868.1 a_0 = 3.378×10^5	97.89%
RMS-Block	b_1 = 368.7, b_0 = -1.458×10^5 a_2 = 1.000, a_1 = 724.3 a_0 = 2.395×10^5	97.45%

each QSG approach. Coefficients of selected TFs along with a statistic showing how well they matched the training data for each PLL including the RMS-block of the MATLAB are summarized in Table IV. Under the change in grid voltage with other ideal grid conditions, the data-driven model for QSGs and the RMS-block performed well with NRMSE fit percentages greater than 97%.

To observe the performance and the impact of each QSG

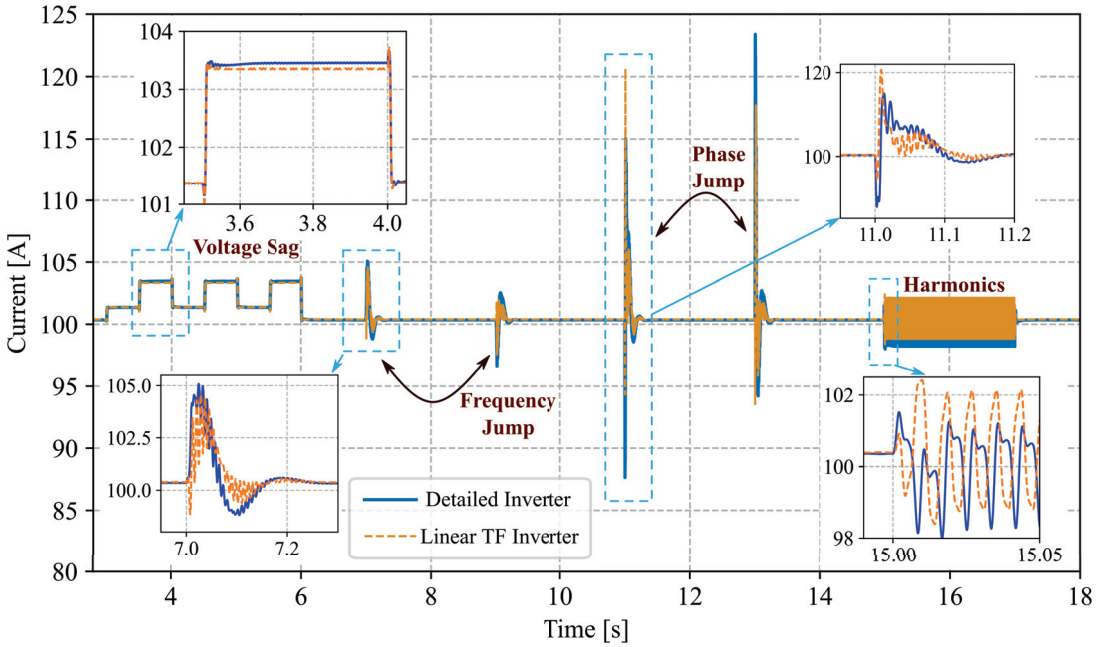

Fig. 8. Simulated output current waveform from derived linear TF model and the detailed GCSI model during the grid events.

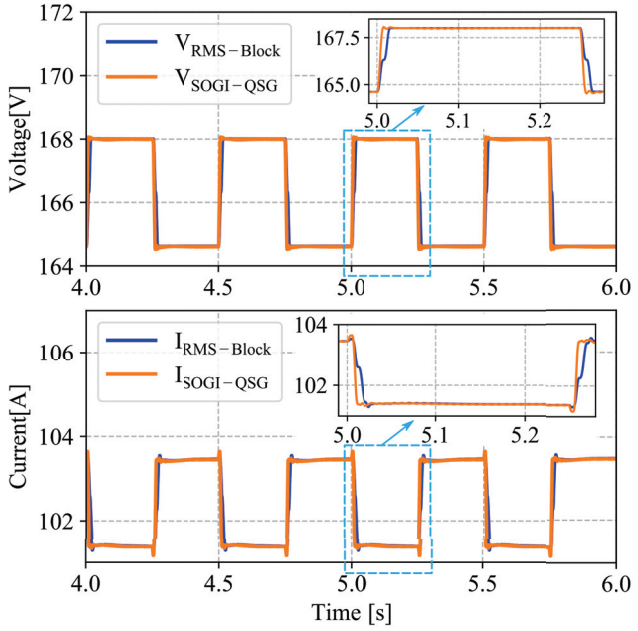

Fig. 9. Peak amplitude of grid voltage (V_g) and inverter output current (I_o) obtained from SOGI-QSG versus the MATLAB RMS-block.

on the selected second-order data-driven models of the GCSI system in realistic grid scenarios, derived models are subjected to the grid disturbances including voltage sag from t = 3 s to 6 s, FV at t = 7 s, and 9 s, PAJ at t = 11 s and t = 13 s, and the harmonic distortion at t = 15 s. Fig. 8 shows the performance of the derived data-driven model for SOGI-QSG, where the model output current in response with the grid-disturbances is compared with the output from the detailed inverter model. The performance is measured and analyzed for each grid disturbance event. The experiment is repeated for each QSG-PLL, including the model developed using the MATLAB RMS-block, as an amplitude extractor and the overall performance in terms of NRMSE fit percentage is shown in Table V. From the results, it is observed that the model derived considering SOGI-QSG outperforms the rest of the approaches during the voltage sag event with cross-validation accuracy of 94.42% (because of the orthogonal signal without any delay), closely followed by the model with APF-QSG. The performance of the model with APF as QSG is observed to be superior to others during the +2 Hz step frequency change with 37.7% (due to the unit gain for all frequencies) followed by RMS-block (30.23%), and SOGI (25.50%). Furthermore, the model with APF as QSG outperformed others during the −40° PAJ with 34.35% followed by RMS-block (28.30%) and SOGI (25.20%). The effect of adding 5% harmonics of the third and fifth order are also investigated, and results show that only the derived model with SFT-QSG tracks the response from the detailed inverter model compared to others with an NRMSE fit percentage of 34.48%. Because of the difficulty in adjusting the LFT and PI due to the presence of two connected non-linear loops, IPT functioned satisfactorily as a QSG.

TABLE V
PERFORMANCE ASSESSMENT OF THE DERIVED TFS OF EACH PLL AND RMS-BLOCK DURING VARIOUS GRID EVENTS.

Grid Events	IPT	SOGI	SFT	APF	RMS-block
Voltage Sag	93.75	94.42	90.76	94.30	92.10
Frequency Jump	22.22	25.50	0	37.70	30.23
Phase Jump	14.45	25.20	17.77	34.35	28.30
Harmonics	0	0	34.48	0	0

V. Conclusions

The purpose of this research is to show how the choice of single-phase QSG-based PLLs affects data-driven GCSI models. The effectiveness of the created model is measured and validated using MATLAB/Simulink in non-ideal grid conditions. In a switched GCSI system, the synchronization block (PLL) is replaced by different QSGs to synchronize and extract the peak value of grid voltage and inverter output current. According to the study, the data-driven model using SOGI as QSG outperformed the others during voltage sag condition. The frequency and phase jump event response of the detailed inverter model is tracked by the APF model. When adding harmonics, only the TF model created for GCSI utilizing SFT was able to track the response of the detailed inverter model, however it failed during the frequency event. It is logical to think that the PLLs employed have an impact on data-driven model performance. It can be concluded that, considering the type of system dynamics and the area under study while selecting PLLs would greatly improve the performance of the data-driven model of the system. When perturbing the system with a square signal while maintaining other ideal grid conditions, second-order TFs were capable of effectively capturing the dynamics; however, exposure of these TFs during non-ideal grid events may be insufficient to capture the dynamics, contributing to the low accuracy. Therefore, we want to study the impact of the estimating model's order on each of these events in the future.

Acknowledgments

The authors would like to thank Nishcal Guruwacharya, Harish Bhandari, and Sheroze Liaquat from SDSU for reviewing the content and their valuable technical input to the paper.

References

[1] "IEEE draft guide for distributed energy resources management systems (DERMS) functional specification," *IEEE*, pp. 1–72, Jan. 2021.

[2] J. Zhang, P. Zhao, Z. Zhang, Y. Yang, F. Blaabjerg, and Z. Dai, "Fast amplitude estimation for low-voltage ride-through operation of single-phase systems," *IEEE Access*, vol. 8, pp. 8477–8484, 2020.

[3] N. Guruwacharya, N. Bhujel, U. Tamrakar, M. Rauniyar, S. Subedi, S. E. Berg, T. M. Hansen, and R. Tonkoski, "Data-driven power electronic converter modeling for low inertia power system dynamic studies," in *2020 IEEE Power Energy Society General Meeting (PESGM)*, 2020, pp. 1–5.

[4] S. Golestan, J. M. Guerrero, and J. C. Vasquez, "Single-phase PLLs: A review of recent advances," *IEEE Transactions on Power Electronics*, vol. 32, no. 12, pp. 9013–9030, 2017.

[5] N. Lokesh and M. K. Mishra, "A comparative performance study of advanced PLLs for grid synchronization," in *2020 IEEE International Conference on Power Electronics, Smart Grid and Renewable Energy (PESGRE2020)*, 2020, pp. 1–6.

[6] J. Xu, H. Qian, S. Bian, Y. Hu, and S. Xie, "Comparative study of single-phase phase-locked loops for grid-connected inverters under non-ideal grid conditions," *CSEE Journal of Power and Energy Systems*, pp. 1–10, 2020.

[7] Q. Zhang, M. Mao, G. Ke, L. Zhou, and B. Xie, "Stability problems of PV inverter in weak grid: a review," *IET Power Electronics*, vol. 13, no. 11, pp. 2165–2174, 2020.

[8] A. Bamigbade, V. Khadkikar, and M. Al Hosani, "Single-phase type-1 frequency-fixed FLL for distorted voltage condition," *IEEE Transactions on Industrial Electronics*, vol. 68, no. 5, pp. 3865–3875, 2021.